Supplementary Information

Contents

1 Supplementary materials and methods

1.1 Antibodies and reagents

Recombinant Mouse CCL3/MIP-1α and blocking Ab against CCL3, CCL4 and CCL5 (anti-CCL4, MAB 451 and AF451; anti-CCL3, MAB450 and AF450; anti-CCL5, MAB478) were from R&D Systems (Minneapolis, MN, USA). Anti-Mouse CD8α (clone 53-6.7, conjugated to PE-Cyanine7 or Alexa-700), anti-Human/Mouse CD44 APC (clone IM7), anti-Mouse CD69 PE-Cyanine7 (clone H1.2F3), anti-Mouse CD25 (clone PC61.5, conjugated to PE-Cyanine7 or APC), unconjugated antibody against T-bet (clone 4B10), anti-Mouse Eomes PerCP-e710 (clone Dan11mag), anti-Mouse IFNγ Biotin (clone XMG1.2), Streptavidin APC, capture antibody against IL-2 (clone JES6-1A12) and detection antibody against IL-2 (clone JES6-5H4) conjugated to APC were all from eBioscience (San Diego, CA, USA). Unconjugated antibody against CyclinD1 (clone 92G2) was from Cell Signaling (Danvers, MA, USA). The polyclonal secondary antibodies APC/Cy7 Goat anti-mouse IgG and APC Goat anti-mouse IgG were from BioLegend (San Diego, CA, USA).

1.2 Measurement of IL-2 concentration in culture supernatant

At each timepoint, culture supernatants were collected and stored at -20°C. 10^7 latex-sulfate beads (4μm diameter, Invitrogen S37225) were washed twice in 1mL MES buffer (25mM, adjusted to pH=7.0 with sulfuric acid) and incubated with 1μg/mL capture antibody against IL-2 (clone JES6-1A12) for 30' at 37°C. Beads were incubated in complete RPMI for 10' at room temperature (RT). Beads were then resuspended in complete RPMI at 2×10^6/mL with 1μg/mL detection Ab against IL-2 (clone JES6-5H4) conjugated to the fluorophore APC and 50μL were distributed per well of a 96 well plate. 50μL of thawed supernatant samples were then added per well and incubated at RT for 1h. Beads were then washed in

FACS buffer and fluoresence was acquired on a LSRII instrument and concentration was estimated using calibration wells with an IL-2 titration.

1.3 Measurement of the absolute number of OT-1 cells

At each time-point, 1/10th (20μL) of the total cell suspension was added to 140μL of FACS buffer containing a viability dye (Live/Dead Yellow, Life Technologies) and fluorophore conjugated antibodies against CD8α (clone 53.6-7). Fluorescence was aquired on a LSRII cytometer at medium speed for at least 60s. The cell density was estimated using the calibrated flow rate of 50uL/min and the absolute number of cells in the initial cell suspension was then calculated.

1.4 Measurement of the percentage of IL-2 producers

The percentage of IL-2 producers was measured using the IL-2 secretion/capture assay by Miltenyi (Auburn, CA). 90μL of the total cell suspension was washed once in 200μL MACS buffer (0.5% bovine serum albumin (BSA), 2 mM EDTA in PBS), resuspended in 50μL MACS buffer containing 1μL of capture Ab and incubated 5' on ice. 200μL of pre-warmed (37°C) complete RPMI was then added and cells were incubated 1h at 37°C on a water bath. Cells were washed once in 200μL MACS buffer and resuspended in 50μL FACS buffer containing a viability dye and fluorochrome conjugated antibodies against IL-2 (clone JES6-5H4) and CD8α (clone 53.6-7). Cells were washed in FACS buffer before fluorescence was acquired on a LSRII instrument.

1.5 Measurement of cell migration

To measure the migration of OT-1 cells in response to chemokine gradients we used transwell permeable supports with 3 μm pore size (Corning Inc. New York, USA, cat. no. 07-200-148) in 24 well plates. OT-1 cells were prepared as described for the signaling assays (see main text). Cells were resuspended in complete RPMI at 10^6/mL. 600μL of complete RPMI containing or not chemokines and/or blocking Abs were added to the bottom well. Cells were harvested and washed once in complete RPMI. 10^5 OT-1 cells in 100 μL were added to the upper well and incubated for 2h at 37°C. The absolute number of OT-1 cells that migrated to the bottom well was then quantified using the protocol described in 1.3.

1.6 Intracellular staining for cytokines

The production of cytokines was measured using the protocol for immunofluorescent staining of intracellular cytokines from BD Biosciences. At the indicated time following initial stimulation, cells were resuspended by pipetting and cytokine extracellular transport was stopped using a protein transport inhibitor (GolgiStop, BD Biosciences, cat. no. 554724.). Cells were then incubated at 37°C for 4h and subsequently stained for surface markers and viability before being fixed and permeabilized by resuspension in the Cytofix/Cytoperm solution for 20' at 4°C. Cells were then washed and incubated at 4°C for 30' in perm/wash buffer containing fluorochrome conjugated antibodies against IL-2 (clone JES6-5H4) and biotinylated antibodies against IFN-γ. Cells were then washed once and incubated at 4°C for 30' in perm/wash buffer containing streptavidin coupled to a fluorescent tag. Cells were washed in FACS buffer before fluorescence was acquired on a LSRII instrument.

1.7 Intracellular staining for transcription factors

The amount of transcription factor was measured using the protocol for staining of intracellular antigens from eBiosciences. At the indicated time following initial stimulation, cells were harvested and stained for surface markers and viability. Cells were then fixed and permeabilized in fixation/permeabilization solution (eBiosciences) for 20' at 4°C. Cells were subsequently washed twice and incubated 20' at RT in permeabilization buffer (eBiosciences) containing primary antibodies against the transcription factor

Tbet and fluorochrome conjugated antibodies against the transcription factor Eomes before being washed and incubated 20' at RT with isotype matched secondary antibodies conjugated with fluorochromes. Cells were washed in FACS buffer before fluorescence was acquired on a LSRII instrument.

2 Description of the model

2.1 TCR signaling

Our model for TCR signaling is an extension of the phenomenological model for early TCR events developed in (François et al., 2013). To account quantitatively for ligand discrimination by the TCR, we consider a generic kinetic proofreading (KPR) cascade supplemented by a negative feedback (see Fig.S4-A). In this framework, the life-time $\tau = 1/\nu$ (note that all parameters are defined in Table 2 in section 2.8) of the complex between the TCR and a given ligand (a peptide bound to a MHC molecule) is the major determinant of the discrimination process. Progression through the different steps of the cascade is controlled by the phosphorylation rate ϕ and the de-phosphorylation rate b. At each step, it is assumed that the complex is immediately de-phosphorylated into unoccupied receptors unpon ligand debinding. Therefore, ligands forming short-lived complexes with the TCR are only allowed to pass a small number of steps while long-lived complexes can progress deeply through the cascade. In the classical KPR scheme with N_p phosphorylation steps, the number of complexes in the final state of the cascade, C_{N_p}, controls the subsequent response and activation. C_{N_p} is shown to scale with N_p according to (McKeithan, 1995):

$$C_{N_p} = C_{tot}\left(\frac{\phi}{\phi+\nu}\right)^{N_p}.$$

At steady state, the total number of complexes, $C_{tot} = \sum_{i=0}^{N_p} C_i$, is a solution of

$$\kappa(A_g - C_{tot})(T - C_{tot}) - \nu C_{tot} = 0 \,\text{that satisfies}\, C_{tot} \leq T,$$

where T is the total number of receptors and A_g the number of ligands. The expression of C_{tot} is therefore given by

$$C_{tot} = \frac{\kappa(T+A_g)+\nu - \sqrt{(\kappa(T+A_g)+\nu)^2 - 4\kappa^2 T A_g}}{2\kappa}.$$

In the particular case of non saturation of the receptors, $T - C_0 - ... - C_N \sim T$ one finds

$$C_{tot} \sim \frac{\kappa T A_g}{\nu + \kappa T}$$

as described in (François et al., 2013).

In the presence of the negative feedback mediated by a phosphatase S, an analytical approximation for C_1 and C_{N_p} as a function of the total number of complexes C_{tot} can be obtained in the limit of strong dissociation constants (for the derivation, see (François et al., 2013)),

$$C_1 \sim C_{tot}\,(1 - r_-)\,r_- \tag{1}$$

and

$$C_{N_p} \sim C_{tot}\left(1 - \frac{r_-}{r_+}\right) r_-^{N_p}$$

where

$$r_\pm = \frac{\phi + b + \gamma S + \nu \pm \sqrt{(\phi + b + \gamma S + \nu)^2 - 4\phi(b+\gamma S)}}{2(b+\gamma S)}.$$

S is the number of active phosphatases given by

$$S = S_{tot}\frac{C_1}{C_1 + C_s} \tag{2}$$

Substituting Eq.(1) into Eq.(2), we obtain a fourth order polynomial equation in S that can be solved numerically and all the other steady state concentrations follow.

In (François et al., 2013), an effective activation threshold K sets the number of C_{N_p} complexes necessary to trigger activation of downstream pathways. We represent on Fig.S4-B the phase diagram of activation as a function of the number of p-MHC ligands and their life-time τ in the presence or absence of the negative feedback. As described in (Altan-Bonnet and Germain, 2005; François et al., 2013), the introduction of a proximal negative feedback enforces a higher selectivity of antigen discrimination without affecting the sensitivity of the response.

Here, rather than a fixed threshold, we consider that C_{N_p} levels continuously control the activation of downstream pathways, possibly in an ultra-sensitive manner (Huang and Ferrell, 1996). Accordingly, we write here the normalized activity of a canonical pathway E downstream of the TCR as:

$$P^{on}_{TCR\to E} = \frac{1}{1+(\frac{K_{TCR\to E}}{C_{N_p}})^{n^{TCR\to E}_{Hill}}}.$$

The signaling processes governing pathway activation are fast compared to those regulating gene expression. The latter processes cannot be considered to be at quasi-equilibrium and approximated by steady-state values. We describe their slow dynamics in the following section.

2.2 Gene expression

Pathways activated downstream of the TCR can regulate the expression of one or multiple target genes (Fig.S4-C). We consider that the rate of transcription of a target gene x is regulated by the activity of different pathways as:

$$\frac{d\ mRNA_X}{dt} = k^{tonic}_X + \sum_E k^{transcription(E)}_X \times P^{on}_{TCR\to E} - k^{degradation}_{mRNA_X} \times mRNA_X$$

where the sum extends over all pathways E for which x is a target gene. For simplicity, we assume here independence between the action of different pathways targeting the same gene. A basal transcription rate k^{tonic}_X is introduced to account for the transcription of gene x in the absence of external stimuli.

Transcripts are then translated into protein X according to:

$$\frac{dX}{dt} = k^{translation}_X \times mRNA_X - k^{degradation}_X \times X$$

These processes are at the origin of an irreducible variability from cell to cell (Lestas et al., 2010). The cell-to-cell variability generated is apparent in the equilibrium distribution of the protein in a population of cells. We simulated these stochastic processes using Gillespies's algorithm (Gillespie, 1976). We represent on Fig.3-B in the main text the equilibrium distribution of IL-2Rα obtained, in absence of external IL-2, for a constant presentation of TCR ligands with different life-times τ using the parameters listed in Table 2 in section 2.8. We also represent the theoretical distribution given by the Gamma distribution (Friedman et al., 2006):

$$P(X) = \frac{X^{A-1}\times e^{-X/B}}{B^A \times \Gamma(A)} \text{ with } A = \frac{k^{tonic}_X + \sum_E k^{transcription(E)}_X \times P^{on}_{TCR\to E}}{k^{degradation}_X} \text{ and } B = \frac{k^{translation}_X}{k^{degradation}_{mRNA_X}}.$$

with Γ denoting the Gamma function. Its mean and coefficient of variation are given by $\langle X\rangle = A\times B$ and $CV(X) = \frac{1}{\sqrt{A}}$ respectively.

2.3 IL-2 signaling

Our model for IL-2 signaling extends the model presented in (Cotari et al., 2013). In (Cotari et al., 2013), a simple thermodynamic model was shown to reproduce quantitatively the effect of different IL-2Rα levels on pSTAT5 EC50 in response to IL-2 stimulation. We find that, provided correlations between

the expression of the different subunits of the IL-2 receptor are introduced, this model can also account for the observed dependency between IL-2Rα expression and pSTAT5 amplitude in response to IL-2 (see Fig.S5-A and B). In the following, we group these different dependencies under IL-2Rα alone and refer to IL-2Rα or IL-2R equivalently. For the sake of simplicity, we recapitulate here the effect of IL-2Rα abundance on pSTAT5 EC50 and amplitude using phenomenological Hill functions (see Fig.S5-A and B). Since phosphorylation of STAT5 is mediated by active JAK kinases, we incorporate the dependencies on IL-2Rα at the level of JAK activity. The normalized activity of the JAK kinases, JAK, as a function of the concentration of IL-2 and of the quantity of IL-2 receptors then reads:

$$JAK = \frac{IL2R}{IL2R + IL2R_0} \times \frac{[IL2]}{[IL2] + EC50_{IL2}(IL2R)}$$

with

$$EC50_{IL2}(IL2R) = EC50^{high}_{IL2} \frac{IL2R}{IL2R + IL2R_0} + EC50^{low}_{IL2} \frac{IL2R_0}{IL2R + IL2R_0}.$$

As C_{N_p} in the case of the TCR, JAK controls the activation of pathways downstream of the IL-2 receptor, in particular the phosphorylation of STAT5 according to:

$$P^{on}_{JAK \to pSTAT5} = \frac{1}{1 + (\frac{K_{JAK \to pSTAT5}}{JAK})^{n^{JAK \to pSTAT5}_{Hill}}}$$

Phosphorylated STAT5 (pSTAT5) regulates the expression of its target genes as described above for TCR activated pathways. In particular, the expression of the *il-2r* gene is regulated both by TCR and IL-2 signals :

$$\begin{aligned} \frac{d\ mRNA_{IL2R}}{dt} &= k^{tonic}_{IL2R} + k^{transcription(TCR)}_{IL2R} \times P^{on}_{TCR \to IL2R} \\ &\quad + k^{transcription(pSTAT5)}_{IL2R} \times P^{on}_{JAK \to pSTAT5} - k^{degradation}_{mRNA_{IL2R}} \times mRNA_{IL2R}. \end{aligned}$$

2.4 Couplings between TCR and IL-2 signals

We present here the implementation of the different coupling mechanisms between IL-2 and TCR pathways included in the complete model (see Fig.S5-D) for IL-2 modulation of cell cycle entry.

TCR impact on IL-2 signaling

TCR signals can impact IL-2 signaling in different ways. Aside from production of IL-2 itself, TCR engagement induces the expression of different subunits of the IL-2 receptor, in particular IL-2Rβ and IL-2Rα (Kalia et al., 2010), thereby enhancing the sensitivity to IL-2. However, it has been reported that TCR activity can also inhibit STAT5 phosphorylation upon IL-2 stimulation by mechanisms that have yet to be identified at the molecular level. We incorporate this inhibitory effect of TCR signals on the activity of JAK as (Tkach et al., 2014):

$$P^{on}_{JAK \to pSTAT5} = \frac{1}{1 + (\frac{K_{JAK \to pSTAT5}}{JAK})^{n^{JAK \to pSTAT5}_{Hill}}} \times (1 - P^{on}_{TCR \to IL2R})$$

TCR inhibition of IL-2 mediated STAT5 phosphorylation impedes the consumption of IL-2 by preventing the efficient induction of IL-2Rα expression by p-STAT5. This inhibition is needed to allow for a greater amount of IL-2 to be accumulated and to reproduce accurately the temporal dynamics of IL-2 accumulation as demonstrated in (Tkach et al., 2014).

PI3K activation

Downstream of the TCR, large signaling complexes are assembled around adapter proteins from where different pathways can branch. Among these pathways, the MAPK and the PI3K pathways can receive parallel inputs from the IL-2 receptor (Reif et al., 1997; Cho et al., 2013).

We have shown that PI3K is a key mediator of the IL-2 modulation of cell cycle entry for weakly stimulated cells. In contrast, even though the MAPK pathway is an important relay of TCR signals, it does not contribute to the observed effect of IL-2 on cell cycle entry (see main text, Fig.2). In order to model the effect of IL-2 on cell cycle entry, we focus in the following on PI3K as a point of convergence for IL-2 and TCR signals for regulation of cell cycle entry.

The normalized activity of the PI3K pathway is therefore controlled both by proximal TCR signals through C_{N_p} and by IL-2 signals via active JAK kinases :

$$P^{on}_{PI3K} = \frac{1}{1+\left(\left(\frac{C_{N_p}}{K_{TCR\rightarrow PI3K}}\right)^{n^{TCR\rightarrow PI3K}_{Hill}} + \left(\frac{JAK}{K_{JAK\rightarrow PI3K}}\right)^{n^{JAK\rightarrow PI3K}_{Hill}}\right)^{-1}}.$$

We use CyclinD1 as a indicator of cell cycle entry whose expression is largely regulated by PI3K activity (Phillips-Mason et al., 2000).

$$\frac{d\ mRNA_{CycD}}{dt} = k^{tonic}_{CycD} + k^{transcription}_{CycD} \times P^{on}_{PI3K} - k^{degradation}_{mRNA_{CycD}} \times mRNA_{CycD}, \tag{3}$$

In agreement with the experimental observation that only cells expressing a high amount of CyclinD1 progress through the cell cycle (see Fig.S2), we consider that a cell starts to divide when its amount of CylinD1 overcomes a given threshold, $CycD \geq CycD^{\star}$.

2.5 Collective regulation of IL-2 and antigen availability

IL-2 dynamics

IL-2 is a shared resource between the large number of cells present (from 10^3 to 10^5). As noted above, the production of IL-2 is controlled by pathways downstream of the TCR. Even though IL-2 signals could impact IL-2 production itself (Villarino et al., 2007), we consider here that IL-2 production is driven only by the pathway E activated downstream of the TCR without contribution from extra inputs from the IL-2 receptor. IL-2 transcripts are produced and degraded according to:

$$\frac{d\ mRNA_{IL2}}{dt} = k^{transcription}_{IL2} \times P^{on}_{TCR\rightarrow IL2} - k^{degradation}_{mRNA_{IL2}} \times mRNA_{IL2}.$$

The instantaneous rate of IL-2 production per cell is given by:

$$\frac{d\,IL2}{dt} = k^{translation}_{IL2} \times mRNA_{IL2}(t) = k^{secretion}_{IL2} \times P^{on}_{TCR\rightarrow IL2} \times \left(1 - e^{-k^{degradation}_{mRNA_{IL2}} \times t}\right) \tag{4}$$

where

$$k^{secretion}_{IL2} = \frac{k^{transcription}_{IL2} \times k^{translation}_{IL2}}{k^{degradation}_{mRNA_{IL2}}}$$

is the maximal production rate per cell. In contrast to CD4+ T cells where the rate of IL-2 secretion can change as function of time increasing when T cells transition from naive precursors to expanding T cells blasts (Huang et al., 2014; Tkach et al., 2014), we find that the rate of IL-2 production per cell is constant for CD8+ T cells (see Fig.S5-C to F). Instead of considering the stochastic production of IL-2 by single cells, we consider its global accumulation by the large number N of cells present and approximate its global instantaneous production rate $\Theta(t)$ using the deterministic solution Eq.(4):

$$\Theta(t) = N \times k^{secretion}_{IL2} \times P^{on}_{TCR\rightarrow IL2} \times \left(1 - e^{-k^{degradation}_{mRNA_{IL2}} \times t}\right)$$

IL-2 degradation is controlled by IL-2 binding to its receptor, internalization and subsequent degradation. IL-2 unbinding from the IL-2 receptor is slow compared to its binding, internalization and subsequent degradation (Tkach et al., 2014). For a cell with $IL2R$ receptors for IL-2, we can then approximate its degradation rate as $k_{IL2}^{on} \times IL2R \times [IL2]$, with k_{IL2}^{on} the on-rate of IL-2 binding to its receptor. The global dynamics of the external concentration of IL-2 is then given by

$$\frac{d\,[IL2]}{dt} = \frac{\Theta(t)}{N_A V} - N \times k_{IL2}^{on} \times IL2R \times [IL2]$$

with N_A the Avogadro number and V the total external volume. $IL2R$ is the average expression of the IL-2 receptor approximated by its deterministic solution as presented above for IL-2. We find that our model accurately reproduces the temporal dynamics of IL-2 accumulation for different initial numbers of cells (see Fig.S5).

Antigen dynamics

As for the external cytokine IL-2, the quantity of antigen available is a resource shared between the large number of cells present. Experimentally, we find that the quantity of antigen available decreases as a function of time in a cell density dependent fashion (see Fig.S4-E and F). We account for this effect by introducing a cell density dependent decay of the number of TCR ligands :

$$\frac{d\,A_g}{dt} = -k_{antigen}^{consumption} \times \frac{N \times N^\star}{N + N^\star} \times A_g$$

with $k_{antigen}^{consumption}$ the maximum rate of ligand consumption per cell reached at low cell density. $N^\star$ accounts for the saturation of the ligand consumption rate at high cell density due to the presence of a finite number of antigen presenting cells.

Impact of P14 and Treg cells

The existence of other cells producing or consuming IL-2 can modify the amount of available external cytokine. We investigate the presence of another population of CD8+ Tcells, P14 cells, whose activation rely on the presence of a different pool of presenting cells bearing the antigen GP_{33-41}. We consider that these cells differ from OT-1 cells only by their TCR. These cells are then simulated using the same model of signaling and gene regulation by TCR and IL-2 pathways as OT-1 cells. Since only the impact of these cells on available IL-2 is considered here, we do not include variables regulating cell cycle entry (See the list of equations in 2.7). We also investigated the suppressive action of Treg cells as pure IL-2 consumer cells. IL-2 consumption is controlled entirely by the expression of the IL-2 receptor. The regulation of IL-2 receptor expression in Treg cells was simulated using the same model as for OT-1 cells at the exception that a high basal expression level was introduced for Treg cells. For a number N_1 of OT-1 cells, N_2 of P14 cells and N_3 of Treg cells, the global regulation of available IL-2 therefore reads:

$$\begin{aligned} d_t[IL2] \quad = \quad & \frac{k_{IL2}^{secretion}}{N_A V}\left(1 - e^{-k_{mRNA_{IL2}}^{degradation} \times t}\right)\left(N_1 \times P_{TCR \to IL2}^{on}(OT1) + N_2 \times P_{TCR \to IL2}^{on}(P14)\right) \\ & -(N_1 \times IL2R(OT1) + N_2 \times IL2R(P14) + N_3 \times IL2R(T_{reg})) \times k_{IL2}^{on} \times [IL2] \end{aligned}$$

The resulting IL-2 dynamics for different number of cells stimulated by different amount of antigen along with the impact of the presence of Treg cells are presented on Fig.S5.

2.6 Numerical simulations

As noted above, the processes regulating gene expression generate variability from cell to cell (Friedman et al., 2006; Lestas et al., 2010). To accurately reproduce the variability in the expression of the IL-2 receptor $IL2R$ and CycD, we simulated these stochastic processes using Gillespie's next reaction algorithm

(Gillespie, 1976). The equations treated as stochastic are indicated in the list of equations in section 2.7. At each step, the next reaction time Δt was determined and the stochastic variables $IL2R$ and $CycD$ were updated accordingly. For deterministic variables, the corresponding equations were integrated using Euler's method with the same time step Δt. For each condition, the percentage of cells that divided was estimated from 10^3 independent simulations.

2.7 List of Equations

Variables for CD8$^+$ OT-1 T cells (i=1)

$$
\begin{aligned}
TCR(i) &= C_{N_p}\left(Ag(i), \tau_i\right) \\
JAK(i) &= \frac{IL2R(i)}{IL2R(i)+IL2R_0} \times \left(1 + \frac{EC50^{high}_{IL2}}{[IL2]} \cdot \frac{IL2R(i)}{IL2R(i)+IL2R_0} + \frac{EC50^{low}_{IL2}}{[IL2]} \frac{IL2R_0}{IL2R(i)+IL2R_0}\right)^{-1} \\
P^{on}_{TCR\to IL2}(i) &= \left(1 + (\frac{K_{TCR\to IL2}}{TCR(i)})^{n^{TCR\to IL2}_{Hill}}\right)^{-1} \\
P^{on}_{TCR\to IL2R}(i) &= \left(1 + (\frac{K_{TCR\to IL2R}}{TCR(i)})^{n^{TCR\to IL2R}_{Hill}}\right)^{-1} \\
P^{on}_{JAK\to pSTAT5}(i) &= \left(1 + (\frac{K_{JAK\to pSTAT5}}{JAK(i)})^{n^{JAK\to pSTAT5}_{Hill}}\right)^{-1} \times (1 - P^{on}_{TCR\to IL2R}(i)) \\
P^{on}_{PI3K}(i) &= \left(1 + \left(\left(\frac{TCR(i)}{K_{TCR\to PI3K}}\right)^{n^{TCR\to PI3K}_{Hill}} + \left(\frac{JAK(i)}{K_{JAK\to PI3K}}\right)^{n^{JAK\to PI3K}_{Hill}}\right)^{-1}\right)^{-1} \\
d_t\, mRNA_{IL2R}(i) &\overset{\text{stoch}}{=} k^{tonic}_{IL2R} + k^{transcription(TCR)}_{IL2R} \times P^{on}_{TCR\to IL2R}(i) \\
&\quad + k^{transcription(pSTAT5)}_{IL2R} \times P^{on}_{JAK\to pSTAT5}(i) - k^{degradation}_{mRNA_{IL2R}} \times mRNA_{IL2R}(i) \\
d_t\, IL2R(i) &\overset{\text{stoch}}{=} k^{translation}_{IL2R} \times mRNA_{IL2R}(i) - k^{degradation}_{IL2R} \times IL2R(i) \\
d_t\, mRNA_{CycD}(i) &\overset{\text{stoch}}{=} k^{tonic}_{CycD} + k^{transcription}_{CycD} \times P^{on}_{PI3K}(i) - k^{degradation}_{mRNA_{CycD}} \times mRNA_{CycD}(i) \\
d_t\, CycD(i) &\overset{\text{stoch}}{=} k^{translation}_{CycD} \times mRNA_{CycD}(i) - k^{degradation}_{CycD} \times CycD(i) \\
d_t Ag(i) &= -k^{consumption}_{antigen} \times \frac{N_i \times N^\star}{N_i + N^\star} \times Ag(i)
\end{aligned}
$$

Variables for CD8$^+$ P14 T cells (i=2)

$$
\begin{aligned}
TCR(i) &= C_{N_p}\left(Ag(i), \tau_i\right) \\
JAK(i) &= \frac{IL2R(i)}{IL2R(i)+IL2R_0} \times \left(1 + \frac{EC50^{high}_{IL2}}{[IL2]} \cdot \frac{IL2R(i)}{IL2R(i)+IL2R_0} + \frac{EC50^{low}_{IL2}}{[IL2]} \frac{IL2R_0}{IL2R(i)+IL2R_0}\right)^{-1}
\end{aligned}
$$

$$
\begin{aligned}
P^{on}_{TCR\to IL2}(i) &= \left(1+(\tfrac{K_{TCR\to IL2}}{TCR(i)})^{n^{TCR\to IL2}_{Hill}}\right)^{-1}\\
P^{on}_{TCR\to IL2R}(i) &= \left(1+(\tfrac{K_{TCR\to IL2R}}{TCR(i)})^{n^{TCR\to IL2R}_{Hill}}\right)^{-1}\\
P^{on}_{JAK\to pSTAT5}(i) &= \left(1+(\tfrac{K_{JAK\to pSTAT5}}{JAK(i)})^{n^{JAK\to pSTAT5}_{Hill}}\right)^{-1}\times(1-P^{on}_{TCR\to IL2R}(i))\\
d_t\, mRNA_{IL2R}(i) &= k^{tonic}_{IL2R}+k^{transcription(TCR)}_{IL2R}\times P^{on}_{TCR\to IL2R}(i)\\
&\quad +k^{transcription(pSTAT5)}_{IL2R}\times P^{on}_{JAK\to pSTAT5}(i)-k^{degradation}_{mRNA_{IL2R}}\times mRNA_{IL2R}(i)\\
d_t\, IL2R(i) &= k^{translation}_{IL2R}\times mRNA_{IL2R}(i)-k^{degradation}_{IL2R}\times IL2R(i)\\
d_t Ag(i) &= -k^{consumption}_{antigen}\times\tfrac{N_i\times N^\star}{N_i+N^\star}\times Ag(i)
\end{aligned}
$$

Variables for Treg cells (i=3)

$$
\begin{aligned}
JAK(i) &= \tfrac{IL2R(i)}{IL2R(i)+IL2R_0}\times\left(1+\tfrac{EC50^{high}_{IL2}}{[IL2]}\cdot\tfrac{IL2R(i)}{IL2R(i)+IL2R_0}+\tfrac{EC50^{low}_{IL2}}{[IL2]}\tfrac{IL2R_0}{IL2R(i)+IL2R_0}\right)^{-1}\\
P^{on}_{JAK\to pSTAT5}(i) &= \left(1+(\tfrac{K_{JAK\to pSTAT5}}{JAK(i)})^{n^{JAK\to pSTAT5}_{Hill}}\right)^{-1}\\
d_t\, mRNA_{IL2R}(i) &= k^{tonic}_{IL2R}(T_{reg})+k^{transcription(pSTAT5)}_{IL2R}\times P^{on}_{JAK\to pSTAT5}(i)\\
&\quad -k^{degradation}_{mRNA_{IL2R}}\times mRNA_{IL2R}(i)\\
d_t\, IL2R(i) &= k^{translation}_{IL2R}\times mRNA_{IL2R}(i)-k^{degradation}_{IL2R}\times IL2R(i)
\end{aligned}
$$

Global regulation of IL-2

$$
\begin{aligned}
d_t[IL2] &= \tfrac{1}{N_A V}\sum_{i=1}^{2}\left(1-e^{-k^{degradation}_{mRNA_{IL2}}\times t}\right)\times k^{secretion}_{IL2}\times N_i\times P^{on}_{TCR\to IL2}(i)\\
&\quad -\sum_{i=1}^{3}k^{on}_{IL2}\times N_i\times IL2R(i)\times[IL2]
\end{aligned}
$$

2.8 List of Parameters

TCR signaling:

$A_g(i)$	$0 - 10^5$	Initial Number of TCR Ligands per cell for i^{th} clone ($i = 1$ for OT–1, $i = 2$ for P14)	(Altan-Bonnet and Germain, 2005)
τ_i	$0.5 - 20s$	Ligand-TCR life-time for i^{th} clone	(François et al., 2013)
ν	$\frac{1}{\tau}$	Ligand-TCR dissociation rate	
κ	$10^{-4}.s^{-1}$	Ligand-TCR association rate	(François et al., 2013)
N_p	5	Number of phosphorylation steps in the KPR cascade	(François et al., 2013)
ϕ	$0.09s^{-1}$	phosphorylation rate	(François et al., 2013)
b	$0.04s^{-1}$	spontaneous dephosphorylation rate	(François et al., 2013)
T	$30,000$	Number of TCR per cell	(François et al., 2013)
S_{tot}	$600,000$	Number of phosphatase per cell	(François et al., 2013)
C_S	500	Threshold for 50% activation of phosphatase	(François et al., 2013)
γ	$1.2 \times 10^{-6}.s^{-1}$	Phosphatase efficiency	(François et al., 2013)
$K_{TCR \to IL2R}$, $K_{TCR \to PI3K}$	0.3	Threshold for activation of pathways downstream of the TCR	This study
$K_{TCR \to IL2}$	0.8	Threshold for activation of IL-2 production downstream of the TCR	This study
$n_{Hill}^{TCR \to IL2R}$, $n_{Hill}^{TCR \to PI3K}$, $n_{Hill}^{TCR \to IL2}$	1	Hill coefficient for activation of pathways downstream of the TCR	This study, note that Hill coefficients above 4 can be reached for some pathways (Huang and Ferrell, 1996)

IL-2 signaling:

$IL2R_0$	2×10^4	Number of IL-2R for 50% of maximal response	This study, adjusted on Fig.S5-A and B
$EC50_{IL2}^{high}$	1 pM	EC50 for high expression of IL-2R	This study, adjusted on Fig.S5-A
$EC50_{IL2}^{low}$	50 pM	EC50 for low expression of IL-2R	This study, adjusted on Fig.S5-A
$K_{JAK \to pSTAT5}$, $K_{JAK \to PI3K}$	0.05	Threshold for activation of downstream pathways by JAK kinases	This study
$n_{Hill}^{JAK \to pSTAT5}$	2	Hill coefficient for activation of STAT5 by JAK	This study, bistability of IL-2R requires values ≥ 2. See also (Busse et al., 2010; Feinerman et al., 2010)
$n_{Hill}^{JAK \to PI3K}$	1	Hill coefficient for activation of PI3K by JAK	This study

IL-2R expression:

$k_{mRNA_{IL2R}}^{degradation}$	$(5h)^{-1}$	Degradation rate of IL-2R transcripts	Set in comparison to other cytokine receptor subunits (Sharova et al., 2009)
$k_{IL2R}^{degradation}$	$(20h)^{-1}$	Degradation rate of of IL-2R	(Duprez and Dautry-Varsat, 1986)
$k_{IL2R}^{transcription(TCR)}$	$10 \times k_{IL2R}^{degradation}$	Rate of transcription of IL-2R downstream of the TCR	Sets $CV(IL2R) \sim 0.3$ (see Fig.S2)
$k_{IL2R}^{translation}$	$10^2 \times k_{mRNA_{IL2R}}^{degradation}$	Rate of translation of IL-2R transcripts	Sets $\langle R \rangle = 10^3$ for agonist ligands (without IL-2) (Tkach et al., 2014; Feinerman et al., 2010)
$k_{IL2R}^{transcription(pSTAT5)}$	$4 \times 10^2 \times k_{IL2R}^{degradation}$	Rate of transcription of IL-2R by pSTAT5	Sets $\langle R \rangle = 4 \times 10^4$ for IL-2 induced maximal expression (Tkach et al., 2014; Feinerman et al., 2010; Cotari et al., 2013)

k_{IL2R}^{tonic}	$0.03 \times k_{IL2R}^{degradation}$	Basal transcription rate of IL-2R	Sets $\langle R \rangle = 3$ in absence of external stimuli
$k_{IL2R}^{tonic}(T_{reg})$	$10 \times k_{IL2R}^{degradation}$	Basal transcription rate of IL-2R for Tregs	Sets $\langle IL2R(T_{reg}) \rangle = 10^3$ in absence of external stimuli for Tregs (Feinerman et al., 2010)

CyclinD1 expression:

$k_{mRNA_{CycD}}^{degradation}$	$(5h)^{-1}$	Degradation rate of CycD transcripts	This study, set equal to $k_{mRNA_{IL2R}}^{degradation}$
$k_{CycD}^{degradation}$	$(20h)^{-1}$	Degradation rate of CycD	This study, sets $\langle t_{start} \rangle \sim 20h$ for agonist ligands (see Fig.4-A and Fig.S2)
$k_{CycD}^{transcription}$	$50 \times k_{CycD}^{degradation}$	Rate of transcription of CycD for maximal PI3K activity	This study, sets $CV(CycD) \sim 0.1$ (see Fig.S2)
$k_{CycD}^{translation}$	$20 \times k_{mRNA_{CycD}}^{degradation}$	Rate of translation of CycD transcripts	This study, sets $\langle CycD \rangle = 10^3$ under maximal PI3K activity
k_{CycD}^{tonic}	$2 \times k_{CycD}^{degradation}$	Basal transcription rate of CycD	This study, sets $\langle CycD \rangle = 100$ in absence of external stimuli
$CycD^{\star}$	500	Threshold on CycD expression for cell cycle entry	This study, set to half of maximal CycD expression (see Fig.S2)

IL-2 production and degradation:

$k_{IL2}^{secretion}$	$60.s^{-1}$	Rate of production of IL-2 molecules per cell	Adjusted on Fig.S5-F, see also (Tkach et al., 2014; Huang et al., 2014)
$k_{mRNA_{IL2}}^{degradation}$	$(5h)^{-1}$	Degradation rate of IL-2 transcripts	(Shim et al., 2002)
k_{IL2}^{on}	$10^7.s^{-1}.M^{-1}$	Association rate of IL-2 and IL-2R	(Duprez and Dautry-Varsat, 1986)

Other parameters:

N_A	$6.02 \times 10^{23} mol^{-1}$	Avogadro number	Universal constant

V	$200\mu L$	Total extracellular volume	Experimental value
N_1	10^5	Number of OT-1 cells	Experimental value
N_2	$0 - 10^5$	Number of P14 cells	Experimental value
N_3	$0 - 10^5$	Number of Treg cells	Experimental value
$N^\star$	10^2	Number of cells for 50% of maximum ligand consumption	This study, see Fig.S4-F
$k_{antigen}^{consumption}$	$\frac{1}{N^\star} \times (5h)^{-1}$	Maximum rate of ligand consumption per cell	This study. Set the time scale of IL-2 production (see Fig.S4-F and Fig.S5)

Table 2: Table of model parameters

Supplementary References

G. Altan-Bonnet and R.N. Germain. Modeling T cell antigen discrimination based on feedback control of digital ERK responses. *PLoS Biol*, 3(11):e356, 2005.

D. Busse, M. de la Rosa, K. Hobiger, K. Thurley, M. Flossdorf, A. Scheffold, and T. Hofer. Competing feedback loops shape IL-2 signaling between helper and regulatory T lymphocytes in cellular microenvironments. *Proc Natl Acad Sci USA*, 107(7):3058–63, 2010.

J. H. Cho, H. O. Kim, K. S. Kim, D. H. Yang, C. D. Surh, and J. Sprent. Unique features of naive CD8+ T cell activation by IL-2. *Journal of Immunology*, 191(11):5559–73, 2013.

J. W. Cotari, G. Voisinne, O. E. Dar, V. Karabacak, and G. Altan-Bonnet. Cell-to-Cell Variability Analysis Dissects the Plasticity of Signaling of Common gamma Chain Cytokines in T Cells. *Science Signaling*, 6(266):ra17–ra17, 2013.

V. Duprez and A. Dautry-Varsat. Receptor-mediated endocytosis of interleukin 2 in a human tumor t cell line. *The Journal of Biochemical Chemistry*, 261(33):15450 – 15454, 1986.

O. Feinerman, G. Jentsch, K. E. Tkach, J. W. Coward, M. M. Hathorn, M. W. Sneddon, T. Emonet, K. A. Smith, and G. Altan-Bonnet. Single-cell quantification of IL-2 response by effector and regulatory T cells reveals critical plasticity in immune response. *Molecular Systems Biology*, 6(1):437, 2010.

P. François, G. Voisinne, E. D. Siggia, G. Altan-Bonnet, and M. Vergassola. A phenotypic model for early T-cell activation displaying sensitivity, specificity and antagonism. *Proc Natl Acad Sci USA*, 110: 888–897, 2013.

N. Friedman, L. Cai, and X. S. Xie. Linking Stochastic Dynamics to Population Distribution: An Analytical Framework of Gene Expression. *Physical Review Letters*, 97:168302, 2006.

D. T. Gillespie. A General Method for Numerically Simulating the Stochastic Time Evolution of Coupled Chemical Reactions. *J Comput Phys*, 22:403–434, 1976.

C. F. Huang and J. E. Ferrell. Ultrasensitivity in the mitogen-activated protein kinase cascade. *Proc Natl Acad Sci USA*, 93:10078–10083, 1996.

J. Huang, M. Brameshuber, X. Zeng, J. Xie, Q. Li, Y. Chien, S. Valitutti, and M. M. Davis. A Single Peptide-Major Histocompatibility Complex Ligand Triggers Digital Cytokine Secretion in CD4+ T Cells. *Immunity*, 39(5):846–857, 2014.

V. Kalia, S. Sarkar, S. Subramaniam, W. N. Haining, K. A. Smith, and R. Ahmed. Prolonged Interleukin-2Rα Expression on Virus-Specific CD8+ T Cells Favors Terminal-Effector Differentiation In Vivo . *Immunity*, 32(1):91 – 103, 2010.

I. Lestas, G. Vinnicombe, and J. Paulsson. Fundamental limits on the suppression of molecular fluctuations. *Nature*, 467(7312):174–178, 09 2010.

T. W. McKeithan. Kinetic proofreading in T-cell receptor signal transduction. *Proc Natl Acad Sci USA*, 92:5042–5046, 1995.

P. J. Phillips-Mason, D. M. Raben, and J. J. Baldassare. Phosphatidylinositol 3-Kinase Activity Regulates α-Thrombin-stimulated G1 Progression by Its Effect on Cyclin D1 Expression and Cyclin-dependent Kinase 4 Activity . *Journal of Biological Chemistry*, 275(24):18046–18053, 2000.

K. Reif, B. M. T. Burgering, and D. A. Cantrell. Phosphatidylinositol 3-Kinase Links the Interleukin-2 Receptor to Protein Kinase B and p70 S6 Kinase. *Journal of Biological Chemistry*, 272(22):14426–14433, 1997.

L. V. Sharova, A. A. Sharov, T. Nedorezov, Y. Piao, N. Shaik, and M. S. H. Ko. Database for mRNA Half-Life of 19 977 Genes Obtained by DNA Microarray Analysis of Pluripotent and Differentiating Mouse Embryonic Stem Cells. *DNA Research*, 16(1):45–58, 2009.

J. Shim, H. Lim, J. R. Yates, and M. Karin. Nuclear Export of NF90 Is Required for Interleukin-2 mRNA Stabilization . *Molecular Cell*, 10(6):1331 – 1344, 2002.

K. E. Tkach, D. Barik, G. Voisinne, N. Malandro, M. M. Hathorn, J. W. Cotari, R. Vogel, T. Merghoub, J. Wolchok, O. Krichevsky, and G. Altan-Bonnet. T cells translate individual, quantal activation into collective, analog cytokine responses via time-integrated feedbacks. *eLife*, 3:e01944, 2014.

A. V. Villarino, C. M. Tato, J. S. Stumhofer, Z. Yao, Y. K. Cui, L. Hennighausen, J. J. O'Shea, and C. A. Hunter. Helper T cell IL-2 production is limited by negative feedback and STAT-dependent cytokine signals. *The Journal of Experimental Medicine*, 204(1):65–71, 2007.

Figure S1 - Impact of different cytokines and chemokines on the proliferation and survival of weakly stimulated CD8+ T cells, Related to Figure 1

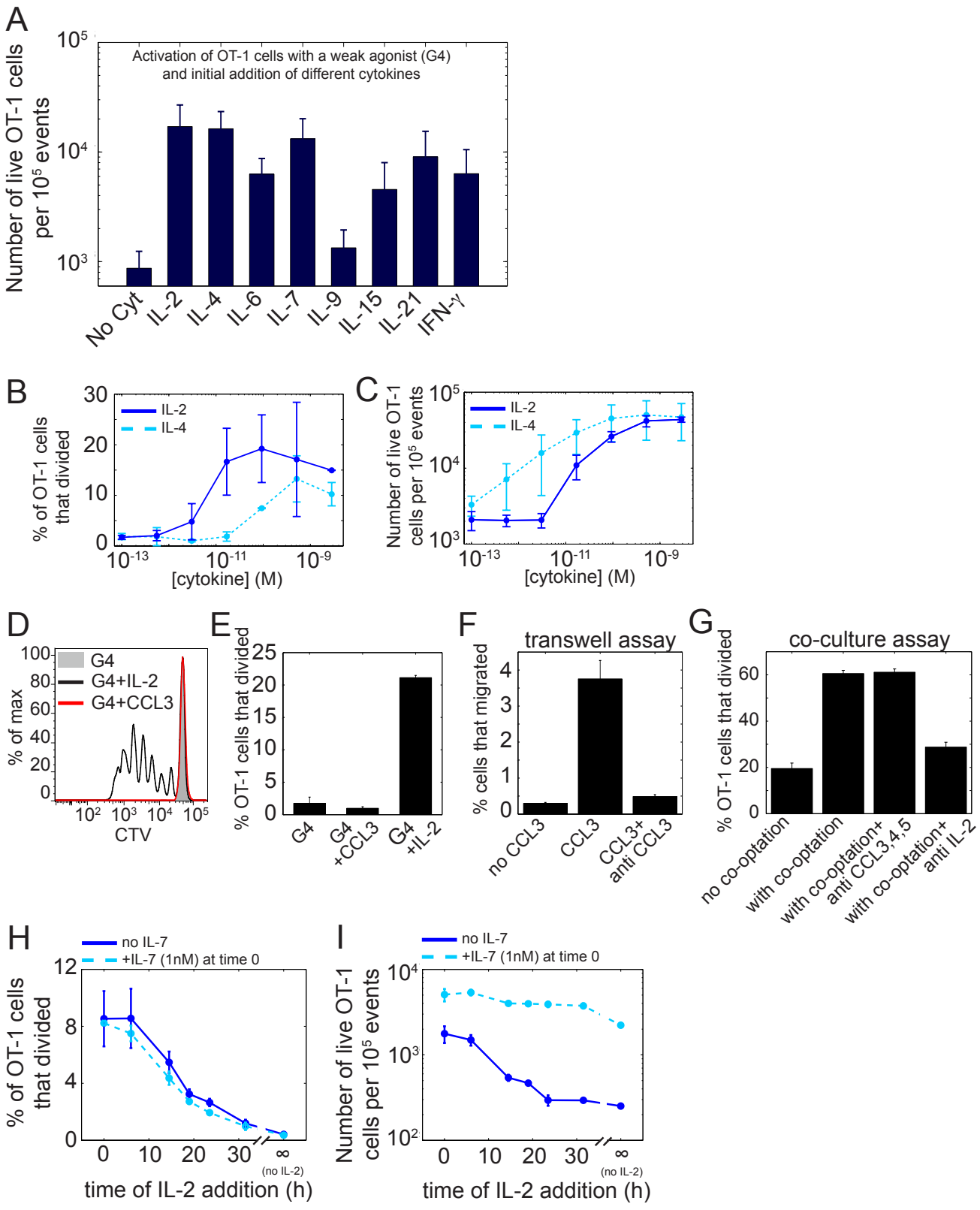

Fig.S1 : (A) Effect of the addition of different cytokines on the survival of OT-1 cells stimulated with the weak agonist G4. A given dose of cytokine (1nM) was added at time t=0 and the number of live OT-1 cells was estimated after 3 days. Error bars represent mean +/- SD for three replicates; the results are representative of n≥3 independent experiments. IL-2 and IL-4 provide equivalent support to the survival of OT-1 cells. Amongst the other cytokines tested, IL-7 was found to be as efficient as IL-2 and IL-4 in promoting cell survival even though it could not trigger cell cycle entry on its own (Fig.1-E).

(B-C) Effect of the initial addition of different doses of the cytokines IL-2 and IL-4 on the proliferation (B) and survival (C) of OT-1 cells stimulated with the weak agonist G4. The number of OT-1 cells that divided and the number of live OT-1 cells was estimated after 3 days. At high doses, IL-2 and IL-4 had comparable effects on the proliferation and survival of weakly stimulated OT-1 cells. Differences emerge when considering the cytokine dose needed to reach half of the maximum response (EC50). For the proliferative response (A), IL-2 had a lower EC50 than IL-4 (~10pM for IL-2 compared to ~100pM for IL-4). The opposite situation is observed when looking at the effect of these cytokines on cell survival. Error bars represent mean +/- SD for two independent experiments

(D-E-F-G). Chemokines are not the mediators of the co-optation of weakly stimulated cells.
(D-E) The chemokine CCL3 cannot trigger proliferation of weakly stimulated CD8+ T cells. CTV stained OT-1 cells were incubated 3 days with G4-pulsed APCs with or without the direct addition of CCL3 (10nM) or IL-2 (1nM) at time zero. (D) Representative histogram of the CTV GMFI for live OT-1 cells. (E) Representation of the percentage of OT-1 precursor cells that divided for the experiment shown in (D). Error bars represent mean +/- SD for three replicates.
(F) Migration of CD8+ T cells in a CCL3 gradient can be abolished using a blocking antibody. 10^5 CD8+ T cells were incubated at 37°C in the upper well of a transwell assay with the bottom well filled with culture media supplemented as indicated ([CCL3]=100pM, [anti CCL3]=1ug/mL). In the condition where the antibody against CCL3 was used, the culture media in the upper well was supplemented with the same concentration of the Ab to guarantee homogeneity of the its concentration. After two hours of incubation, the absolute number of CD8+ cells in the bottom well was measured by flow cytometry and the percentage of cells that migrated was then calculated. Error bars represent mean +/- SD for two replicates; the results are representative of n≥2 independent experiments.
(G) Chemokines are not involved in T cell co-optation *in vitro*. OT-1 cells were stimulated with a weak agonist (G4) in presence of P14 cells left either unstimulated (‘no co-optation‘) or stimulated by their cognate antigen GP33-41 (‘with co-optation‘). Blocking antibodies against the chemokines CCL3, CCL4 and CCL5 and the cytokine IL-2 were added at time t=0. As compared to IL-2 blockade, blocking chemokines does not limit cooptation of weakly stimulated T cells. Error bars represent mean +/- SD for three replicates; the results are representative of n≥2 independent experiments.

(H-I) IL-2 is needed early after TCR stimulation independently of cell death.
Effect of the addition of IL-2 at different times after TCR stimulation with the weak agonist G4. A given dose (1nM) of IL-2 was added at the indicated times after incubation of OT-1 with G4-pulsed APCs with or without the initial addition of IL-7 (1nM). The number of naïve OT-1 cells that entered cell division and the number of live OT-1 cells was estimated 3 days after the initial incubation. As expected from the previous results (A, Fig.1-E), the addition of IL-7 promoted cell survival (I) without triggering cell proliferation on its own (H, see condition ‘no IL-2’). We observed that IL-2 addition was needed in the first 20 hours following TCR stimulation, irrespectively of the presence of IL-7. Thus, the observed time dependence on IL-2 addition is not due to overall cell death. Error bars represent mean +/- SD for two replicates; the results are representative of n≥2 independent experiments.

Figure S2 - Activation profile for CD8+ T cells as a function of time, antigen quality, and the presence of IL-2, Related to Figure 1 and Figure 3

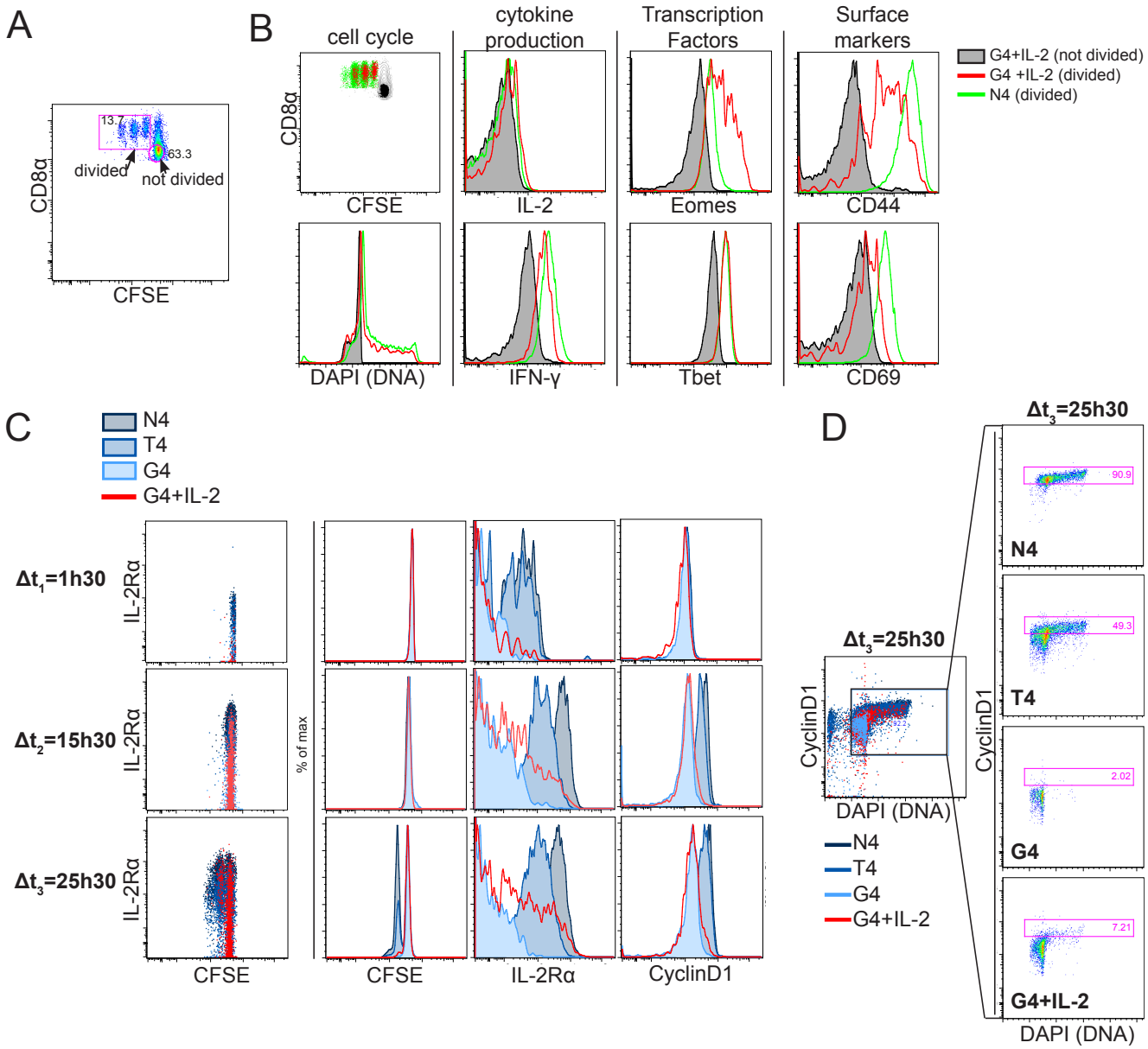

Fig.S2 : (A-B) Comparison of activation profiles between strongly stimulated CD8+ T cells in absence of IL-2 and weakly stimulated CD8+ T cells in presence of IL-2. CFSE stained OT-1 cells were incubated 3 days with APCs pulsed with the indicated peptides in the presence of a blocking antibody against the endogenous mouse IL-2 (clone JES6-1A12) either alone or with the addition of an initial dose (1nM) of human IL-2 (condition indicated with '+IL-2').

(A) Dot plot representing the GMFI of CFSE and CD8α for OT-1 cells stimulated with G4 in presence of IL-2. Gates for non-activated cells (gate 'not divided', $CD8\alpha^{low}.CFSE^{high}$) and activated cells that divided at least once (gate 'divided', $CD8\alpha^{high}.CFSE^{low}$) are represented.

(B) After 3 days of incubation, collected cells were split into four groups ('cell cycle', 'cytokine production', 'transcription factors' and 'surface markers') and subsequently treated and stained for different activation markers according to the corresponding protocol (see Material and Methods). Dot plots or histograms of GMFI values are represented on each plot for the 'not divided' and 'divided' populations of weakly stimulated cells in presence of IL-2 ('G4+IL-2') and strongly stimulated cells in absence of IL-2 ('N4').

Under both types of stimulation, activated cells (gate 'divided') had similar profiles in terms of cell cycle and

cytokine production markers. However, activated cells originating from weakly stimulated cells in presence of IL-2 expressed intermediate amounts of the surface markers CD44 and CD69. In addition, these cells showed similar induction of the transcription factor Tbet and greater induction of the transcription factor Eomes.

(C-D) Kinetics of IL-2Rα and CyclinD1 expression as a function of antigen quality.
(C) IL-2Rα expression, CyclinD1 expression and cell cycle progression as a function of time and antigen quality. CFSE stained OT-1 CD8+ T cells were stimulated with antigens of varied strength (N4 > T4 > G4). Cells were cultured for 3 days in the presence of a blocking antibody against the endogenous mouse IL-2 (clone JES6-1A12) either alone ('No Cyt') or with the addition of an initial dose (1nM) of human IL-2. Dot plots and histograms of the GMFI of CFSE and IL-2Rα at different times following stimulation are presented. At different times following stimulation, Expression of IL-2Rα and CyclinD1 increases as a function of time and antigen quality. From Δt_1=1h30 to Δt_2=15h30 after stimulation, IL-2Rα expression was slightly up-regulated in weakly stimulated cells in absence of IL-2. Presence of IL-2 allowed a fraction of these cells to express amounts of IL-2Rα comparable to those reached by more potently stimulated cells (with T4 or N4). At Δt_3=25h30, a first division peak is present in the histogram of CFSE. While a large part of strongly stimulated cells had divided at this time, amongst weakly stimulated cells in presence of IL-2, only a reduced fraction of cells expressing high quantities of IL-2Rα had entered cell cycle.

(D) Dot plots of the GMFI of CyclinD1 and DAPI at Δt3=25h30 after stimulation are presented. High DAPI fluorescence indicates progression through the S and G2 phases of the cell cycle. Only cells that accumulated enough CyclinD1 progress through the cell cycle. For weakly stimulated cells, only the presence of IL-2 allows the accumulation of enough cyclinD1 to enter cell cycle.

Figure S3 - PI3K mediates cell cycle entry but not IL-2 mediated IL-2Rα upregulation, Related to Figure 2

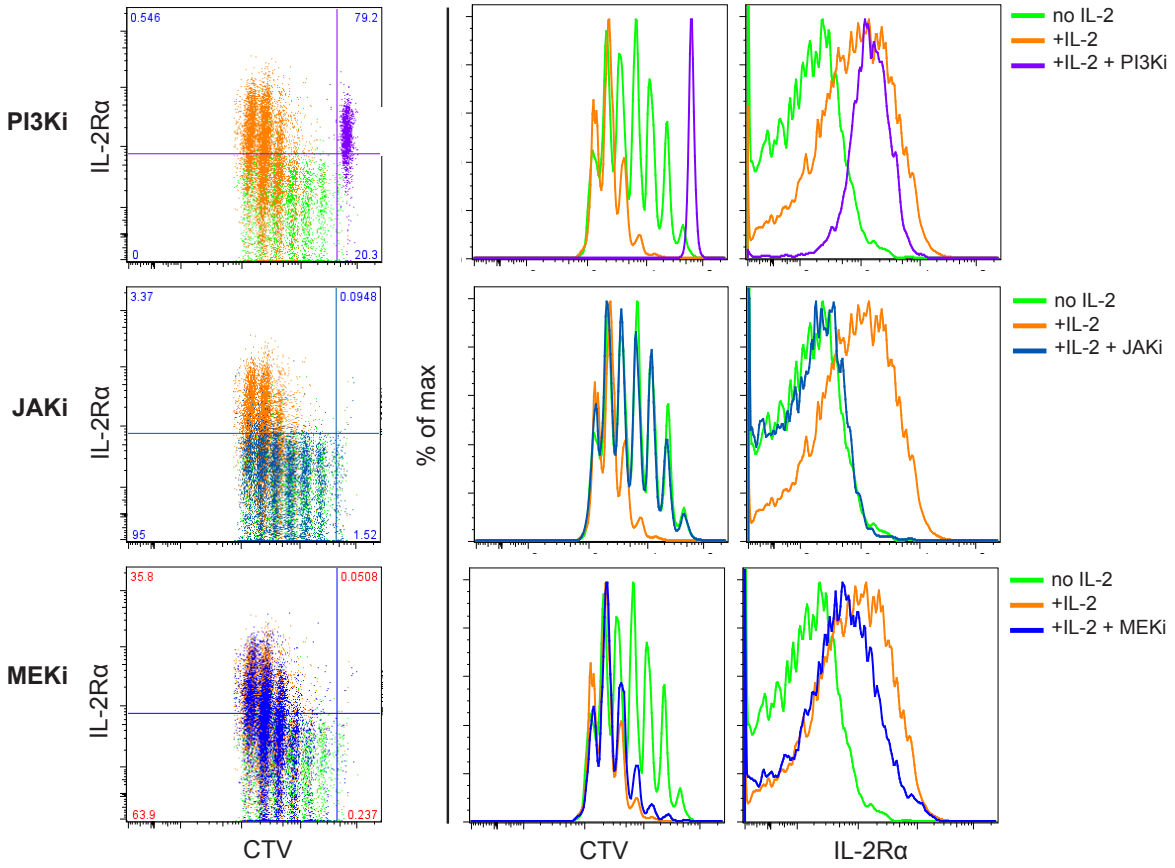

Fig.S3 : Impact of small molecule inhibitors on proliferation and IL-2Rα expression. CTV stained OT-1 cells were incubated 3 days with APCs pulsed with 1uM of the intermediate agonist T4 in the presence of a blocking antibody against the endogenous mouse IL-2 (clone PC61) either alone or with the addition of an initial dose (1nM) of human IL-2 (condition indicated with '+IL-2') and different inhibitors (MEKi : 1uM, JAKi : 1uM, PI3Ki : 50uM). The data are from the same experiment as on Fig.2-D at the exception of the higher concentration of PI3K inhibitor shown here. Dot plots and histograms of the GMFI of CTV and IL-2Rα for the different conditions of stimulation are presented. For this TCR stimulation of intermediate strength, cell cycle entry was delayed in the absence of IL-2 (as quantified on Fig.2-E). Inhibition of PI3K prevented progression into the cell cycle but didn't prevent IL-2 mediated upregulation of IL-2Rα. JAK inhibition abrogated IL-2 effects entirely both on cell cycle progression and IL-2Rα expression whereas MEK1/2 inhibition interfered little on the impact of IL-2.

Figure S4 - Details of the model for antigen discrimination by CD8+ T cells, Related to Figure 3 and Figure 4

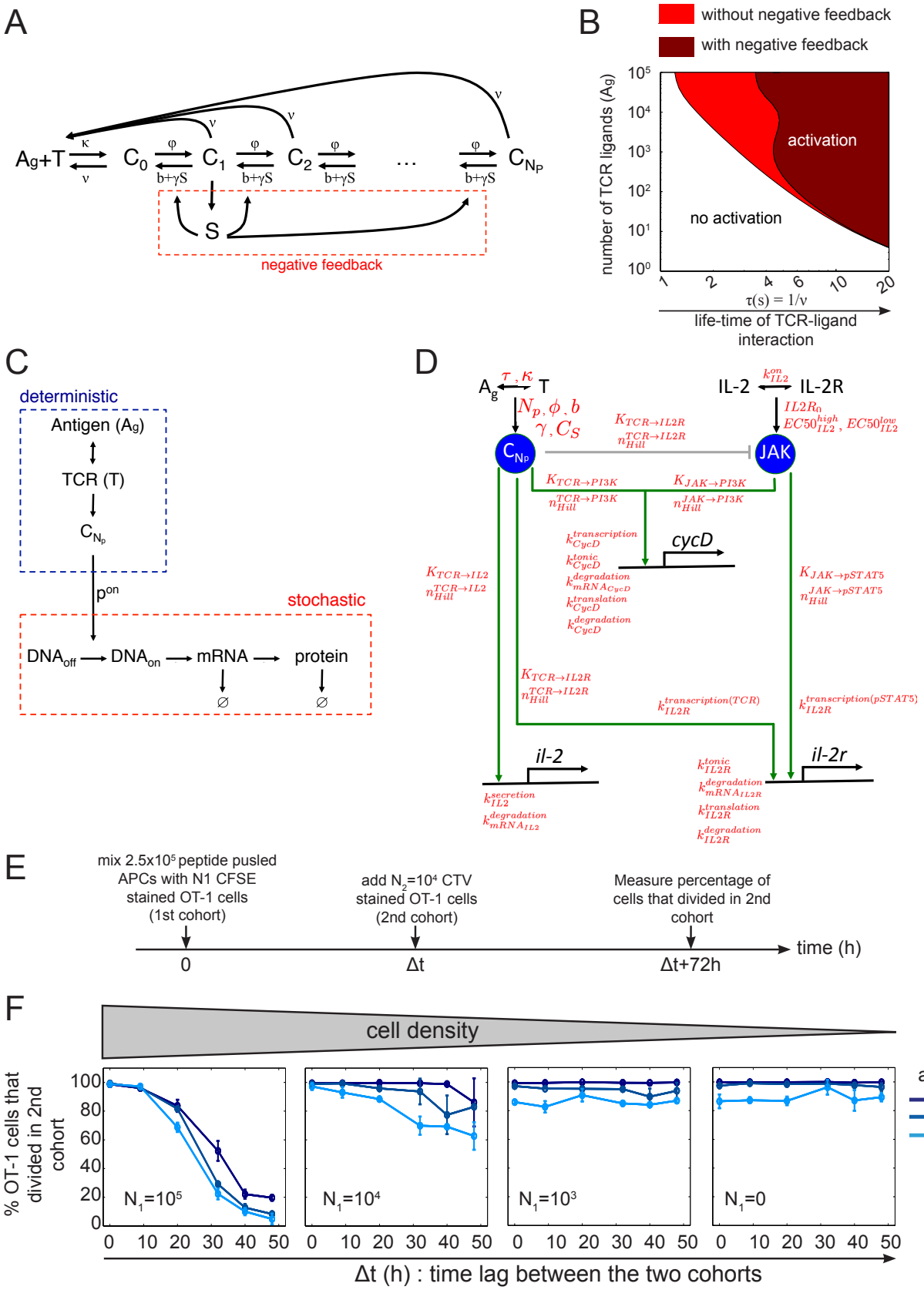

Fig.S4 : (A-B) Model for antigen discrimination at the level of early TCR events.
(A) Schematic of the model for antigen discrimination by the TCR (as in (François et al., 2013)). (B) Phase diagram of activation as a function of the number of TCR ligands and the life-time of TCR-ligand interaction $\tau=1/v$ for a fixed threshold on C_{N_P} (K=0.2 as in (François et al., 2013)). The impact of the negative feedback mediated by the phosphatase S is represented.

(C) Schematic of the model for the regulation of gene expression for a pathway downstream of the TCR. The fast signaling events are treated as deterministic while the slow processes of gene regulation are treated as stochastic. These processes are responsible for an irreducible variability in protein abundance between individual cells.

(D) Schematic of the full model integrating TCR and IL-2 signals for the control of cell cycle entry. The signaling state of the TCR and IL-2 pathways are represented by the activity of their proximal components C_{N_P} and JAK respectively (in blue). These components regulate the transcriptional activity of different downstream pathways represented in green and pointing towards their respective target genes. Model parameters are represented in red and placed in proximity to the corresponding process.

(E-F) Antigen availability as a function of time and cell density. (E) To test for antigen availability as a function of time, we used two cohorts of cells. A first cohort of N_1 OT-1 cells was incubated with peptide pulsed APCs. After a time Δt, a second cohort of $N_2=10^4$ CTV stained OT-1 cells was added. As a proxy for the quantity of antigen remaining available at time Δt, the percentage of cells that divided in the second cohort was measured three days after their addition.
(F) Representation of the percentage of cells that divided in the second cohort three days after their addition as a function of the lag time Δt between the stimulation of the two cohorts of cells. The number of cells that divided in the second cohort depended strongly on the number of cells N_1 in the first cohort. This is consistent with a cell density dependent antigen decay (suggesting antigen trogocytosis).

Figure S5 - IL-2 signaling and dynamics as a function of cell number, quantity of antigen and presence of Tregs, Related to Figure 3 and Figure 5

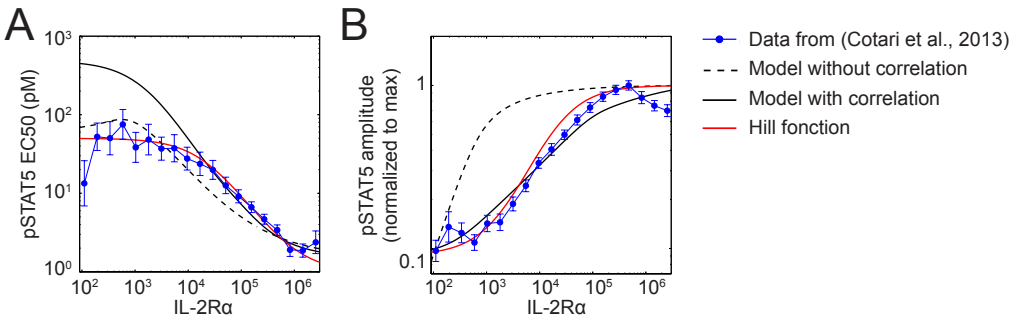

experiments

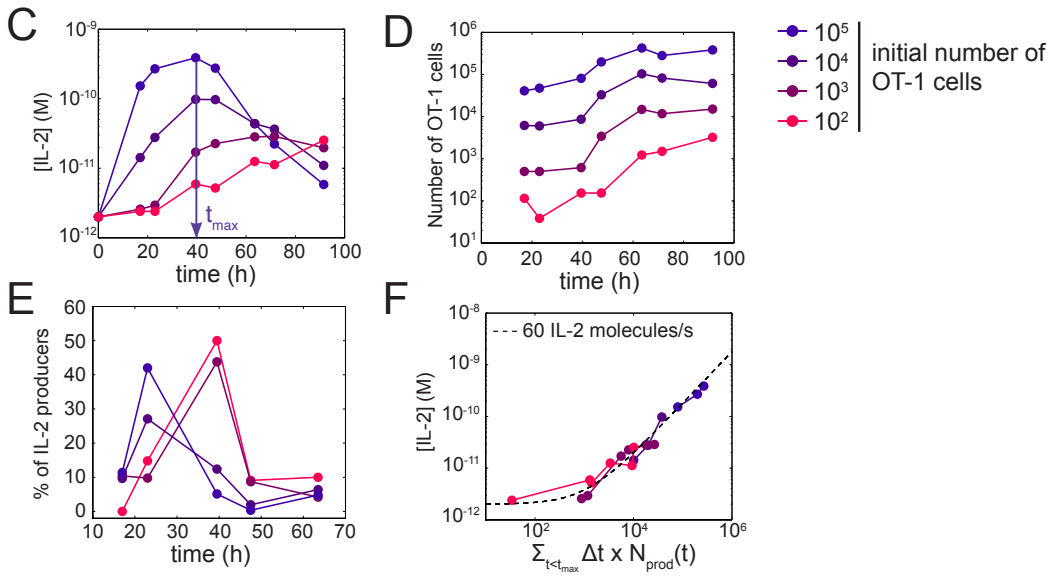

model

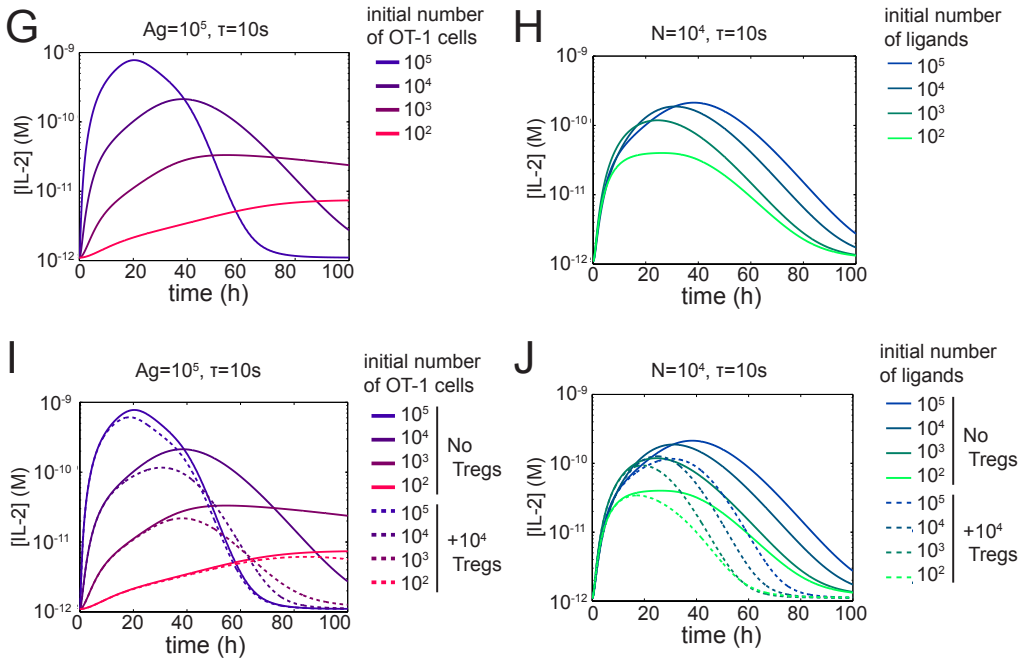

Fig.S5 : (A-B) IL-2 signaling depends on IL-2Rα expression.
Representation of the EC50 (A) and amplitude (B) for IL-2 induced STAT5 phosphorylation as a function of IL-2Rα abundance. The experimental results and the model for the dependence of pSTAT5 EC50 on IL-2Rα expression are taken from Cotari et al, 2013.The same data is used to plot pSTAT5 amplitude as a function of IL-2Rα expression. The model from Cotari et al can reproduce the dependence of pSTAT5 amplitude on IL-2Rα expression when correlations between the expressions of IL-2Rα and the other subunits (IL-2Rβ and γc) of the IL-2 receptor are introduced. For simplicity, in the present model for IL-2 signaling, the dependency of pSTAT5 EC50 and amplitude on IL-2Rα abundance are modeled phenomenologically using Hill fits of the experimental data (represented in red).

(C-D-E-F) IL-2 dynamics and estimation of IL-2 production rate.
(C-E) Representation of the concentration of IL-2 (C), the absolute number of OT-1 cells (D) and the percentage of IL-2 producing cells amongst OT-1 cells (E) as a function of time following stimulation for different initial number of OT-1 cells. OT-1 cells were stimulated by $2.5x10^5$ APCs pulsed with 1uM of the agonist N4.
(F) Representation of the concentration of IL-2 as a function of the cumulated number of IL-2 producers (same data as in (A-C)) until the time when the maximal aount of IL-2 is reached (represented on (C) for one condition). The slope of this curve gives the rate of IL-2 production per cell. We represent the concentration of IL-2 as a function of the cumulated number of IL-2 producers for a constant production rate of 60 IL-2 molecules/s per cell (dashed black line). Note that a background at $\sim 10^{-12}$ M is added to account for the detection limit of the ELISA assay.

(G-H-I-J) IL-2 dynamics as a function of cell number, quantity of antigen and presence of Tregs.
(G-H) Representation of the theoretical concentration of IL-2 as a function of time for different initial numbers of T cells (G) stimulated by different amount (H) of a strong agonist (τ=10s). (I-J) Impact of the presence of 10^4 Tregs cells on the accumulation of IL-2 for the same conditions as presented in (G-H). Tregs cells limit both the maximal amount of IL-2 accumulated and the duration of the presence of IL-2 above a given level.